

# Realizing High Efficiency over 20% of Low-Bandgap Pb–Sn-Alloyed Perovskite Solar Cells by In Situ Reduction of Sn<sup>4+</sup>

Tingming Jiang, Zeng Chen, Xu Chen, Tianyu Liu, Xinya Chen, Wei E. I. Sha, Haiming Zhu, and Yang (Michael) Yang\*

Although the theoretical power conversion efficiency (PCE) of low-bandgap Pb–Sn-alloyed perovskite solar cells (PSCs) is higher than that of its conventional pure Pb counterpart, its device performance currently has been severely restricted by the large open-circuit voltage ( $V_{oc}$ ) loss. Herein, it is discovered that the Sn<sup>4+</sup>-induced trap states of the perovskite film can be effectively suppressed by introducing excess Sn powder into the precursor solution (FASnI<sub>3</sub>) to reduce the Sn<sup>4+</sup> content. As a result, the average charge carrier lifetime of the perovskite film increases remarkably from 115 to 701 ns due to the suppressed nonradiative recombination, and the energy levels have up-shifted by about 0.27 eV, rendering a more favorable energy-level alignment at the interface. Ultimately, the champion PSCs using a low-bandgap (FASnI<sub>3</sub>)<sub>0.6</sub>(MAPbI<sub>3</sub>)<sub>0.4</sub> perovskite film with Sn<sup>4+</sup> reduction show a high  $V_{oc}$  of 0.843 V corresponding to a  $V_{oc}$  loss as low as 0.397 eV and a high fill factor of 80.34%, leading to an impressive PCE of 20.7%, which is one of the few instances of a PCE over 20% for low-bandgap mixed Pb–Sn PSCs to date.

(1.7–1.9 eV) and a low-bandgap bottom cell (1.1–1.3 eV) with a predicted maximum PCE over 40%.<sup>[16,17]</sup> In addition to the tandem cell, the Sn–Pb-alloyed perovskite with a more suitable bandgap of  $\approx 1.24$  eV has a higher theoretical efficiency limit for a single-junction cell.

Many efforts have been devoted to improving the PCE of low-bandgap mixed Pb–Sn PSCs.<sup>[18–28]</sup> However, it often exhibits a larger open-circuit voltage ( $V_{oc}$ ) loss, and therefore, its efficiency is far behind that of pure Pb-based PSCs with a medium bandgap. It is worth to note that Yan and Zhu et al. recently used guanidinium thiocyanate (GuaSCN) additive to passivate the grain boundaries and substantially reduce the defect density in mixed Pb–Sn perovskite films, leading to a high PCE over 20%, which is the first report for mixed Pb–Sn PSCs with PCEs over 20%.<sup>[12]</sup> The

The highest certified power conversion efficiency (PCE) of PSCs has reached 25.2%<sup>[1]</sup> for organic–inorganic halide perovskite solar cells (PSCs) with a medium bandgap of  $\approx 1.5$  eV, approaching its Shockley–Queisser (S–Q) limit.<sup>[2]</sup> A proven method to break the S–Q limit is to fabricate perovskite–perovskite tandem solar cells,<sup>[3–17]</sup> which combines a wide-bandgap front cell

larger  $V_{oc}$  loss of low-bandgap mixed Pb–Sn PSCs is likely associated with two factors: 1) the high trap density of the perovskite film, resulting in severe nonradiative recombination, and 2) an unsuitable energy-level alignment between perovskite film and charge transport layers.<sup>[15,27,29–31]</sup> It is believed that the Sn<sup>4+</sup> acts as p-type dopants in the Pb–Sn-alloyed perovskite films which induce deep trap states to boost nonradiative recombination.<sup>[32–34]</sup> Unfortunately, even a highly purified commercial starting material SnI<sub>2</sub> (99.9%, trace metal) could contain up to 10 wt% of SnI<sub>4</sub> due to the technical difficulty of the complete removal of Sn<sup>4+</sup> during the synthesis, as reported by Wakamiya and coworkers recently.<sup>[35]</sup> In addition, even though the storage of the starting material SnI<sub>2</sub> and the preparation of Sn-based perovskite films is carried out under a N<sub>2</sub>-filled glove box, it is impossible to completely prevent oxygen exposure, so a certain degree of oxidation of Sn<sup>2+</sup> to Sn<sup>4+</sup> is still likely to occur during that time.

Therefore, in this work, we reported an in situ Sn<sup>4+</sup> reduction method by adding excess Sn powder into the formamidinium tin iodide (FASnI<sub>3</sub>) precursor solution during its dissolution process. With the help of the heating treatment of the precursor solution, the redox reaction Sn<sup>4+</sup> + Sn  $\rightarrow$  2Sn<sup>2+</sup> is triggered,<sup>[36]</sup> and the Sn<sup>4+</sup> content is considerably reduced. The trap density of the film has decreased significantly from  $7 \times 10^{14}$  to  $4.34 \times 10^{14}$  cm<sup>-3</sup>, and the average charge carrier lifetime of

Dr. T. Jiang, X. Chen, T. Liu, X. Chen, Prof. Y. (Michael) Yang  
 State Key Laboratory of Modern Optical Instrumentation  
 College of Optical Science and Engineering  
 Zhejiang University  
 Zheda Road, Hangzhou 310027, China  
 E-mail: yangyang15@zju.edu.cn

Z. Chen, Prof. H. Zhu  
 Department of Chemistry  
 Center for Chemistry of High-Performance & Novel Materials  
 Zheda Road, Hangzhou 310027, China

Prof. W. E. I. Sha  
 Key Laboratory of Micro-nano Electronic Devices and Smart Systems of  
 Zhejiang Province  
 College of Information Science and Electronic Engineering  
 Zhejiang University  
 Zheda Road, Hangzhou 310027, China

 The ORCID identification number(s) for the author(s) of this article can be found under <https://doi.org/10.1002/solr.201900467>.

DOI: 10.1002/solr.201900467

the film has increased remarkably from 115 to 701 ns due to the reduced defect density and trap-assisted recombination. In addition, the valence band maximum (VBM) has up-shifted from  $-5.89$  to  $-5.62$  eV, making the energy-level alignment at the perovskite/hole-transport layer interface more suitable. Finally, the champion device fabricated by the  $\text{Sn}^{4+}$  reduction method delivers a high PCE of 20.7% with a large  $V_{oc}$  of 0.843 V corresponding to a remarkable low  $V_{oc}$  loss of 0.397 eV, whereas the best control device without  $\text{Sn}^{4+}$  reduction exhibits a  $V_{oc}$  of 0.795 V, fill factor (FF) of 75.82%, and PCE of 17.39%. The PCE of 20.7% achieved in this work is one of the highest reported PCEs for low-bandgap mixed Pb–Sn PSCs to date.

To identify the reduction effect of Sn powder on  $\text{Sn}^{4+}$ , X-ray photoelectron spectroscopy (XPS) has been conducted. Figure 1a, b shows XPS Sn  $3d_{5/2}$  spectra for the perovskite films without and with  $\text{Sn}^{4+}$  reduction, separately. Both spectra can be decomposed into one dominant component and a small peak with a higher binding energy. The main component (black line) with a binding energy at about  $486.4 \pm 0.05$  eV is assigned with  $\text{Sn}^{2+}$ , whereas the smaller peak (green line) locating at about  $487.5 \pm 0.05$  eV is attributed to  $\text{Sn}^{4+}$  ions, which are in good agreement with previous reports.<sup>[37,38]</sup> It is obvious that the intensity of  $\text{Sn}^{4+}$  component in the film with  $\text{Sn}^{4+}$  reduction is significantly lower than the one without  $\text{Sn}^{4+}$  reduction. The XPS result shows direct evidence that the addition of Sn powder into the  $\text{FASnI}_3$  solution has effectively reduced  $\text{Sn}^{4+}$

to a lower degree. We further estimated the trap density values of the perovskite films without and with the Sn powder reduction effect using the space-charge-limited-current (SCLC) method.<sup>[39]</sup> The electron-only devices are fabricated by adopting the configuration ITO/ $\text{SnO}_2$ /( $\text{FASnI}_3$ )<sub>0.6</sub>( $\text{MAPbI}_3$ )<sub>0.4</sub>/ $\text{C}_{60}$ /Ag, and the dark  $J$ - $V$  characteristics have been measured and are shown in Figure 1c,d for devices without and with  $\text{Sn}^{4+}$  reduction. The linear region at low bias voltage represents an ohmic contact, and a marked increase in the current injection appears as the increase in bias voltage at the intermediate region, which is identified as the trap-filling process. The kink point between the two regions is defined as the trap-filling limit voltage ( $V_{TFL}$ ), so trap density can be calculated from the following equation<sup>[39,40]</sup>

$$V_{TFL} = eL^2N_{\text{trap}}/2\epsilon\epsilon_0 \quad (1)$$

where  $e$  is the electron elementary charge,  $\epsilon$  stands for the relative dielectric constant,  $\epsilon_0$  represents the vacuum permittivity, and  $L$  is the thickness of the perovskite films. The  $V_{TFL}$  values for devices without and with  $\text{Sn}^{4+}$  reduction are confirmed to be 0.626 and 0.388 V, respectively, as shown in Figure 1c,d. The electron trap density of the device with  $\text{Sn}^{4+}$  reduction is then calculated to be  $4.34 \times 10^{14} \text{ cm}^{-3}$ , which is much lower than that ( $7 \times 10^{14} \text{ cm}^{-3}$ ) of the device without  $\text{Sn}^{4+}$  reduction. The reduced trap density is clearly attributed to the decreased amount

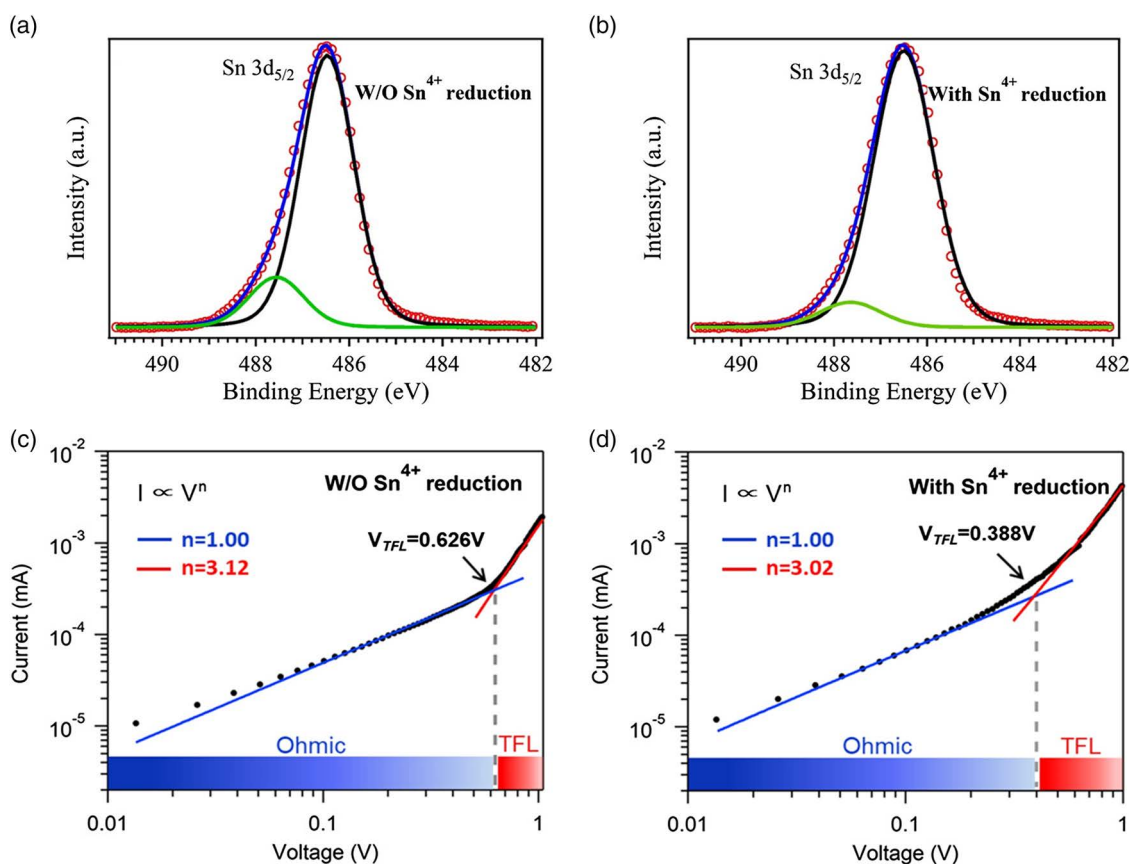


**Figure 1.** High-resolution XPS spectra of the Sn  $3d_{5/2}$  region for the ( $\text{FASnI}_3$ )<sub>0.6</sub>( $\text{MAPbI}_3$ )<sub>0.4</sub> perovskite films a) without and b) with  $\text{Sn}^{4+}$  reduction. Trap density evaluation of perovskite films c) without and d) with  $\text{Sn}^{4+}$  reduction using dark  $J$ - $V$  curve measurements of the electron-only devices.

of  $\text{Sn}^{4+}$  in the mixed Pb–Sn perovskite films, which is ascribed to the Sn powder reduction effect.

**Figure 2** shows the top-view SEM images of  $(\text{FASnI}_3)_{0.6}(\text{MAPbI}_3)_{0.4}$  perovskite films without and with Sn powder reduction, respectively. Perovskite films in both cases are compact and pinhole free with some grain sizes reaching over 1  $\mu\text{m}$ . However, the proportion of crystal grains with sizes over 1  $\mu\text{m}$  for perovskite film with  $\text{Sn}^{4+}$  reduction seems slightly higher than that of the film without  $\text{Sn}^{4+}$  reduction. Note that it has proven difficult to synthesize uniform, pinhole-free, and Sn-based perovskite thin films because Sn-based perovskite films crystallized rapidly, the thickness of the  $(\text{FASnI}_3)_{0.6}(\text{MAPbI}_3)_{0.4}$  perovskite films prepared in this work is about 800 nm which is thicker than most previous reports of mixed Pb–Sn PSCs.<sup>[19–21,23]</sup> It seems that the average grain size of the film is comparable with the film thickness. Thicker films with larger grains are favorable for fabricating  $(\text{FASnI}_3)_{0.6}(\text{MAPbI}_3)_{0.4}$  PSCs to attain enhanced external quantum efficiencies (EQEs) in the infrared wavelength region, which is important for bottom cell in tandem solar cells. The crystallization of  $(\text{FASnI}_3)_{0.6}(\text{MAPbI}_3)_{0.4}$  films on PEDOT:PSS without and with  $\text{Sn}^{4+}$  reduction has been evaluated by X-ray diffraction (XRD) measurements, as shown in Figure S1, Supporting Information. The two XRD patterns show strong diffraction peaks at  $14.1^\circ$  and  $28.3^\circ$  corresponding to (110) and (220) preferred orientation.<sup>[13,19]</sup> There is no obvious change in the XRD patterns of the perovskite films without and with  $\text{Sn}^{4+}$  reduction, which indicates that Sn powder reduction has little effect on the crystallization of  $(\text{FASnI}_3)_{0.6}(\text{MAPbI}_3)_{0.4}$  perovskite films.

**Figure 3a** shows the optical absorption spectra of  $(\text{FASnI}_3)_{0.6}(\text{MAPbI}_3)_{0.4}$  perovskite films without and with  $\text{Sn}^{4+}$  reduction, which are almost identical. The optical bandgaps of the perovskite films are estimated to be as low as about 1.24 eV by fitting the  $(\alpha h\nu)^2$ -E plot, as shown in Figure S2, Supporting Information. To access the reduction effect of Sn powder on the photophysical property of perovskite films, we measured the steady-state photoluminescence (PL) and time-resolved photoluminescence (TRPL) decay of the  $(\text{FASnI}_3)_{0.6}(\text{MAPbI}_3)_{0.4}$  perovskite films without and with  $\text{Sn}^{4+}$  reduction deposited on pristine glass. As shown in Figure 3b, the PL intensity of perovskite films with  $\text{Sn}^{4+}$  reduction is about 2.5 times larger than that of films without  $\text{Sn}^{4+}$  reduction, indicating that the trap states are reduced in the perovskite films with  $\text{Sn}^{4+}$  reduction. To evaluate the electronic quality of the mixed

Pb–Sn perovskite films, we have calculated the Urbach energies by combining emission and absorption spectra, as shown in Figure S3, Supporting Information. The Urbach energy of the perovskite film with  $\text{Sn}^{4+}$  reduction is about 14.2 meV, which is relatively lower than that (17 meV) of the film without  $\text{Sn}^{4+}$  reduction, also demonstrating a lower density of trap states in the film.<sup>[13,41]</sup> From the TRPL spectra shown in Figure 3c, the spectra of perovskite films without and with  $\text{Sn}^{4+}$  reduction are well fitted with the single-exponential function, indicating that the perovskite films we prepared have reasonably good electronic quality required for photovoltaic operation. The average charge carrier lifetime of perovskite film has increased drastically from 115 to 701 ns by Sn powder reduction effect. Such a remarkably long carrier lifetime for low-bandgap mixed Pb–Sn perovskite is even comparable with that of Pure Pb perovskites.<sup>[41,42]</sup> A longer carrier lifetime indicates a lower nonradiative recombination rate associated with reduced trap states in the perovskite films, which is supposed to lead to a high  $V_{oc}$  for the PSCs. The enhanced PL intensity and significantly prolonged charge carrier lifetime of the perovskite film with  $\text{Sn}^{4+}$  reduction are certainly attributed to the decreased defects due to the reduction of  $\text{Sn}^{4+}$  compared with that of the film without  $\text{Sn}^{4+}$  reduction, in line with the analysis of XPS, SCLC measurements for trap density, and calculated Urbach energies. In addition, the longer charge carrier lifetime of the perovskite film with  $\text{Sn}^{4+}$  reduction is also consistent with the micron-sized crystal grains with less grain boundaries because grain boundaries can act as recombination centers and charge carrier traps. For low-bandgap mixed Pb–Sn PSCs, one critical issue that remained is the low spectral response in the infrared region which restricts the further increase in short-circuit current density ( $J_{sc}$ ). This is primarily due to the relative thin ( $\approx 400$  nm) film thickness, resulting in insufficient absorption of infrared solar photons. Simply increasing the thickness of the mixed Pb–Sn perovskite film cannot guarantee the increase in  $J_{sc}$  if the excited carriers cannot last long enough to get collected. Based on the aforementioned results, we have successfully synthesized thick ( $\approx 800$  nm) low-bandgap mixed Pb–Sn  $(\text{FASnI}_3)_{0.6}(\text{MAPbI}_3)_{0.4}$  perovskite films with sufficiently long charge carrier lifetimes, which are promising to achieve both high  $V_{oc}$  and  $J_{sc}$ .

To investigate if the  $\text{Sn}^{4+}$  reduction has an effect on the energy levels of the perovskite films, we have carried out ultraviolet photoelectron spectroscopy (UPS) measurement to determine the VBM and CBM. The UPS spectra including onset ( $E_i$ ) and cutoff ( $E_{cutoff}$ ) energy region are shown in Figure 3d,e. According to the

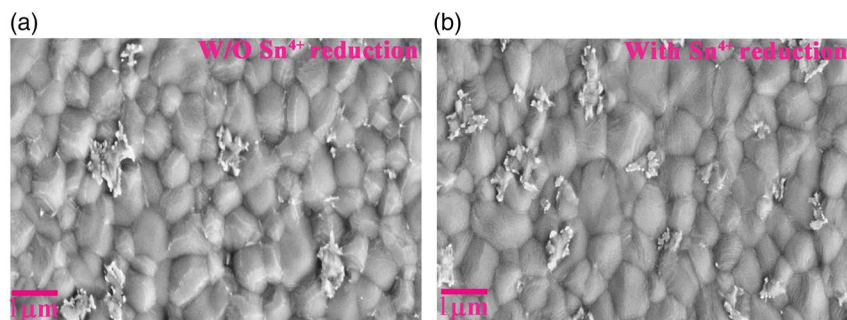


**Figure 2.** Top-view SEM images of mixed Pb–Sn perovskite films a) without and b) with  $\text{Sn}^{4+}$  reduction.

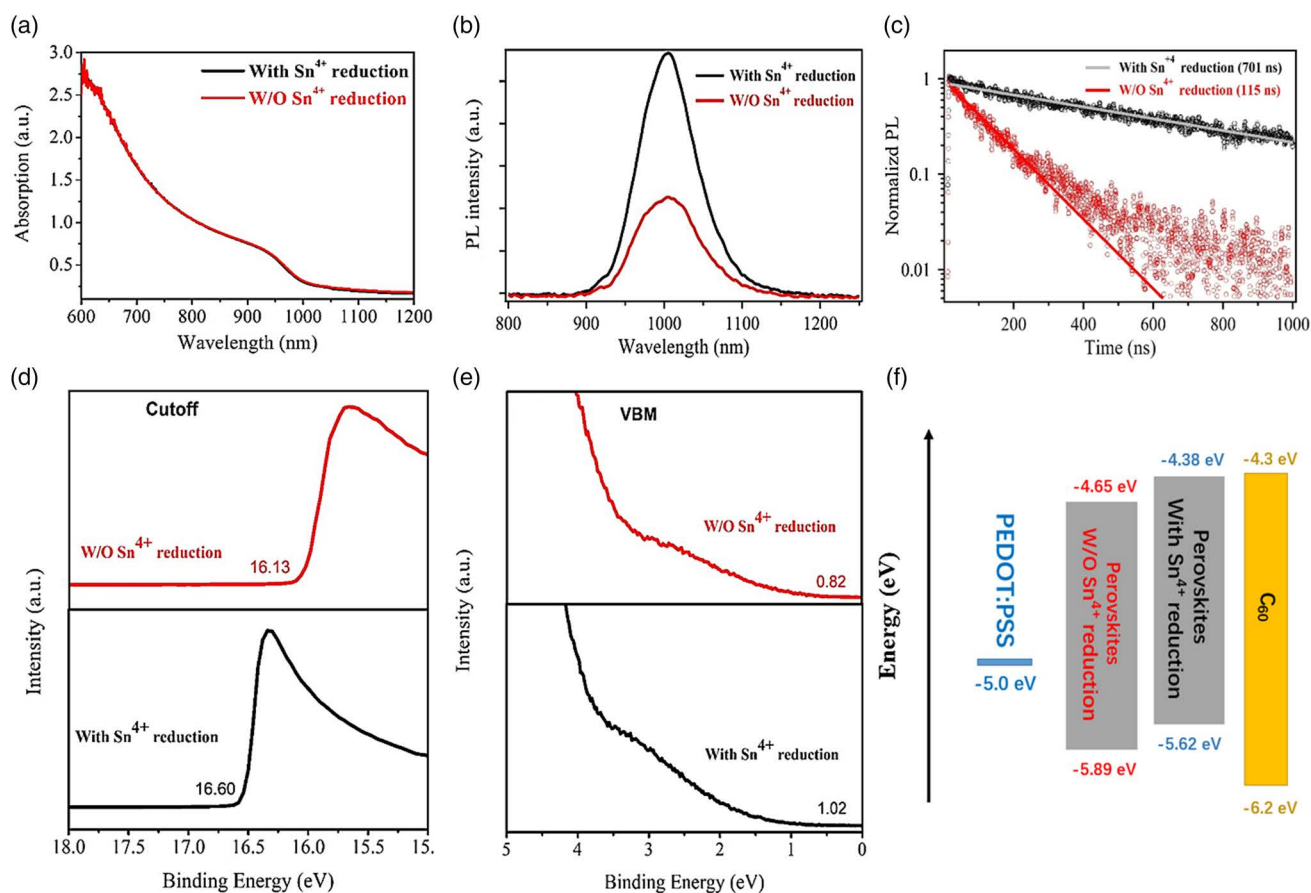


**Figure 3.** a) UV-vis absorption spectra of (FASnI<sub>3</sub>)<sub>0.6</sub>(MAPbI<sub>3</sub>)<sub>0.4</sub> perovskite films without and with Sn<sup>4+</sup> reduction. b) Steady-state PL spectra of perovskite films without and with Sn<sup>4+</sup> reduction deposited on glass. c) Time-resolved PL decay of perovskite films without and with Sn<sup>4+</sup> reduction. UPS spectra in the d) cutoff and e) onset energy region for perovskite films without and with Sn<sup>4+</sup> reduction. f) Energy-level diagrams of corresponding materials.

equation<sup>[43]</sup>  $E_{\text{VBM}} = 21.2 - (E_{\text{cutoff}} - E_i)$ , the VBM and CBM of perovskite film without Sn<sup>4+</sup> reduction are determined to be -5.89 and -4.65 eV. As shown in Figure 3f, the VBM and CBM of the perovskite film with Sn<sup>4+</sup> reduction are up-shifted to -5.62 and -4.38 eV, respectively, which form more energetically favorable interfaces at perovskite/PEDOT:PSS and perovskite/C<sub>60</sub>. The improved proper energy-level alignment also contributes to the efficient collection of the photogenerated carriers and leads to a higher  $V_{\text{oc}}$  and FF of a low-bandgap (FASnI<sub>3</sub>)<sub>0.6</sub>(MAPbI<sub>3</sub>)<sub>0.4</sub> PSCs.

The solar cell devices are fabricated by adopting the inverted p-i-n architecture, as shown in Figure 4a, composed of glass /ITO /PEDOT:PSS / (FASnI<sub>3</sub>)<sub>0.6</sub>(MAPbI<sub>3</sub>)<sub>0.4</sub> /C<sub>60</sub> /BCP /Ag. Figure 4b shows the current density-voltage ( $J$ - $V$ ) curves of the devices using (FASnI<sub>3</sub>)<sub>0.6</sub>(MAPbI<sub>3</sub>)<sub>0.4</sub> perovskite films without and with Sn<sup>4+</sup> reduction in forward scan direction. The highest PCE of devices based on perovskite films without Sn<sup>4+</sup> reduction is 17.39% with a  $V_{\text{oc}}$  of 0.795 V,  $J_{\text{sc}}$  of 28.85 mA cm<sup>-2</sup>, and FF of 75.82%, whereas for the champion device using perovskite films with Sn<sup>4+</sup> reduction, the  $V_{\text{oc}}$ ,  $J_{\text{sc}}$ , and FF are significantly improved to 0.843 V, 30.58 mA cm<sup>-2</sup>, and 80.34%, respectively, leading to an impressively high PCE

of 20.7%. To the best of our knowledge, this is one of the few PCEs over 20% reported to date for low-bandgap mixed Pb-Sn PSCs. We deem the significant enhancement of  $V_{\text{oc}}$  and FF for the device using perovskite film with Sn<sup>4+</sup> reduction as a result of the remarkably prolonged charge carrier lifetime of the perovskite film and better energy-level alignment between perovskite film and charge transport layers. The comparison of the  $J$ - $V$  curve in both forward and reverse scan is shown in Figure S4, Supporting Information, with corresponding photovoltaic parameters inside. It is noteworthy to mention that the high  $J_{\text{sc}}$  (over 30 mA cm<sup>-2</sup>) of champion device with Sn<sup>4+</sup> is reasonably attributed to the thick perovskite film (800 nm) with a substantially long charge carrier lifetime because the thick low-bandgap mixed Pb-Sn perovskite film can absorb more solar photons especially in the infrared region, and the photo-generated charge carriers have sufficient lifetime to travel a longer distance to be collected. The EQEs of the solar cells have also been measured, as shown in Figure 4c. The two spectra both demonstrate a broad spectral response extending to 1050 nm, in line with the optical absorption results. For the device with Sn<sup>4+</sup> reduction, the EQEs reach up to 80% in the near-infrared range of 700–850 nm, which is of great significance for the bottom cell

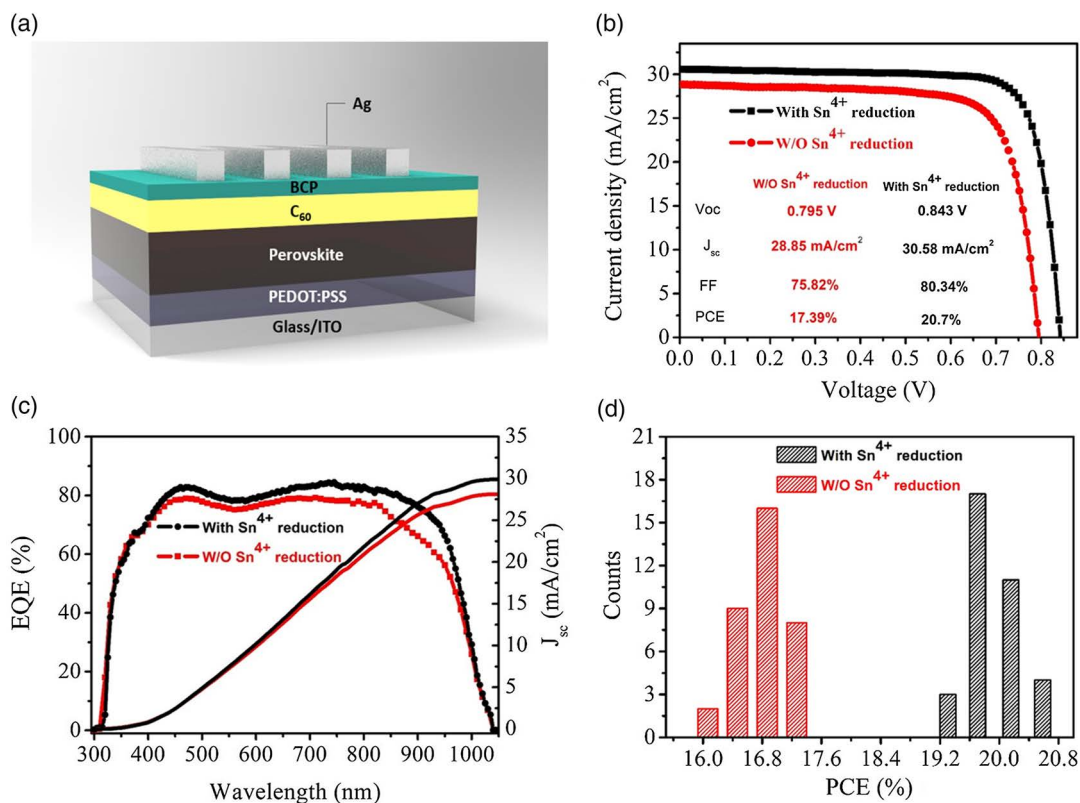


**Figure 4.** a) Schematic of device architecture of inverted PSCs. b)  $J$ - $V$  curves of PSCs based on  $(\text{FASnI}_3)_{0.6}(\text{MAPbI}_3)_{0.4}$  perovskite films without and with  $\text{Sn}^{4+}$  reduction under  $100 \text{ mW cm}^{-2}$  AM 1.5G illumination under forward scan. c) EQE spectra (left axis) and integrated  $J_{\text{sc}}$  (right axis) of PSCs without and with  $\text{Sn}^{4+}$  reduction. d) Histograms of PCEs for devices without and with  $\text{Sn}^{4+}$  reduction.

in a perovskite tandem device. The integrated  $J_{\text{sc}}$  from the EQE spectra for devices without and with  $\text{Sn}^{4+}$  reduction is 28.12 and 29.89  $\text{mA cm}^{-2}$  respectively, which match well with those obtained from the  $J$ - $V$  characteristics. Figure 4d shows the histogram of PCE distribution of 35 devices based on perovskite film without and with  $\text{Sn}^{4+}$  reduction, which indicates a high reproducibility of a high PCE for device with  $\text{Sn}^{4+}$  reduction. In addition, the device stability is also studied, as shown in Figure S5, Supporting Information, and the unencapsulated device with  $\text{Sn}^{4+}$  reduction has been kept in the  $\text{N}_2$ -filled glovebox for over 2 months ( $\text{H}_2\text{O} < 0.1 \text{ ppm}$ ,  $\text{O}_2 < 1 \text{ ppm}$ ) and was occasionally measured under one sun illumination ( $100 \text{ mW cm}^{-2}$ ). The PCE drop is less than 5%, indicating that the phase of mixed Pb-Sn perovskite is stable during storage. In addition, we have investigated the  $\text{Sn}^{4+}$  reduction effect based on a different amount of Sn powder and a different reaction time. Figure S6 and S7, Supporting Information, show the  $J$ - $V$  curves of devices (forward and reverse scan), SEM images, and XRD patterns of perovskite films using 0.05 and 0.1 g Sn powder under different reaction times: 1 h, 2 h, and 4 h. The PCEs of these devices under different conditions all reach over 20% (forward scan), and the corresponding SEM images as well as XRD patterns exhibit little variation. These results indicate that the reduction level of  $\text{Sn}^{4+}$  is barely affected by the amount of tin powder added and the reaction time.

A modified detailed balance model<sup>[26,44]</sup> is used to simulate the experimental  $J$ - $V$  curves to understand the PCE loss mechanism

of our low-bandgap mixed Pb-Sn PSCs. The simulated  $J$ - $V$  curves can provide three primary parameters including the non-radiative recombination rate  $\gamma$ , the series resistance  $R_s$ , and the shunt resistance  $R_{\text{sh}}$ .  $R_s$  is associated with ohmic loss, and  $R_{\text{sh}}$  is an indication of defects and current leakage. Figure 5 shows the fitted and experimental  $J$ - $V$  curves of PSCs without and with  $\text{Sn}^{4+}$  reduction with  $\gamma$ ,  $R_s$ , and  $R_{\text{sh}}$  parameters. It is noticeable that the nonradiative recombination rate  $\gamma$  for the device with  $\text{Sn}^{4+}$  reduction is about 2.5 times lower than that of the device without  $\text{Sn}^{4+}$  reduction, which is consistent with the long charge carrier lifetime of the perovskite film and a low  $V_{\text{oc}}$  loss of 0.397 V. The smaller  $R_s$  and larger  $R_{\text{sh}}$  of device with  $\text{Sn}^{4+}$  reduction compared with the device without  $\text{Sn}^{4+}$  reduction indicate lower interfacial ohmic loss and defect-induced current leakage, which corresponds well with trap density evaluation and energy-level modification results shown by XPS, SCLC, and UPS analysis. The dark  $I$ - $V$  curves of the solar cells without and with  $\text{Sn}^{4+}$  reduction have also been measured, as shown in Figure S8, Supporting Information. The device with  $\text{Sn}^{4+}$  reduction shows lower dark current at negative and positive bias voltages compared with the device without  $\text{Sn}^{4+}$  reduction, suggesting improved charge transport and decreased recombination loss in the device,<sup>[45]</sup> which is also in line with the reduced non-radiative recombination rate  $\gamma$ . The results of simulations by the modified detailed balance model and dark  $I$ - $V$  characteristics have further confirmed that the reduction of  $\text{Sn}^{4+}$  by Sn powder has substantially reduced the trap density of the mixed Pb-Sn

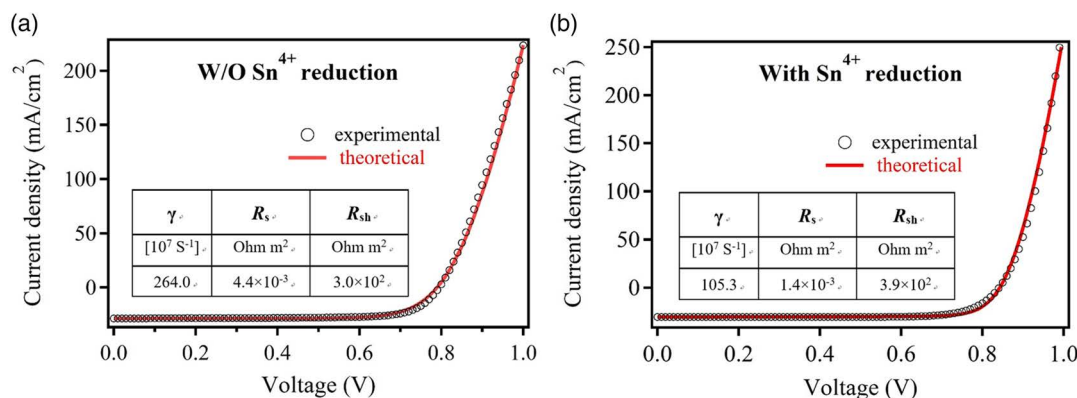


**Figure 5.** The theoretical and experimental  $J$ - $V$  characteristics of PSCs a) without and b) with  $\text{Sn}^{4+}$  reduction.

perovskite films and finally led to the outstanding device performance of low-bandgap mixed Pb-Sn PSCs.

In summary, we prepared low-bandgap mixed  $(\text{FASnI}_3)_{0.6}(\text{MAPbI}_3)_{0.4}$  perovskite films by adding excess highly purified Sn powder into the Sn-containing precursor  $\text{FASnI}_3$  and effectively reduced the parasitic  $\text{Sn}^{4+}$  to  $\text{Sn}^{2+}$ . The reduction effect of Sn powder is evidenced by the XPS measurement. The trap density of the perovskite film with  $\text{Sn}^{4+}$  reduction is reduced substantially, as proved by the SCLC measurement and the calculated Erbach energy. The nonradiative recombination of perovskite film with  $\text{Sn}^{4+}$  reduction has been drastically suppressed, which leads to a remarkably long charge carrier lifetime of 701 ns. In addition, the energy levels of the perovskite film with  $\text{Sn}^{4+}$  reduction have up-shifted by about 0.27 eV, which preferably match the energy levels of charge transport layers (PEDOT: PSS and  $\text{C}_{60}$ ). Consequently, the champion solar cell using the perovskite film with  $\text{Sn}^{4+}$  reduction shows a high  $V_{oc}$  of 0.843 V,  $J_{sc}$  of  $30.58 \text{ mA cm}^{-2}$ , and FF of 80.34%, compared with  $V_{oc}$  of 0.797 V,  $J_{sc}$  of  $28.85 \text{ mA cm}^{-2}$ , and FF of 75.82% for the best control device without  $\text{Sn}^{4+}$  reduction. Our work offers a simple and effective method to further improve the PCE of low-bandgap Pb-Sn mixed PSCs

## Supporting Information

Supporting Information is available from the Wiley Online Library or from the author.

## Acknowledgements

T.J. and Z.C. contributed equally to this work. The authors acknowledge the support from the National Key Research and Development Program of China (2017YFA0207700), Outstanding Youth Fund of Zhejiang Natural Science Foundation of China (LR18F050001), and Natural Science Foundation of China (61804134).

## Conflict of Interest

The authors declare no conflict of interest.

## Keywords

low bandgap, mixed Pb-Sn perovskite solar cells, open-circuit voltage loss,  $\text{Sn}^{4+}$  reduction

Received: October 22, 2019

Revised: November 25, 2019

Published online: December 5, 2019

- [1] NREL, Research Cell Record Efficiency Chart, <https://www.nrel.gov/pv/cell-efficiency.html> (accessed: October 2019).
- [2] W. Shockley, H. J. Queisser, *J. Appl. Phys.* **1961**, 32, 510.
- [3] I. Celik, A. B. Phillips, Z. Song, Y. Yan, R. J. Ellingson, M. J. Heben, D. Apul, *Energy Environ. Sci.* **2017**, 10, 1874.
- [4] F. Hao, C. C. Stoumpos, R. P. H. Chang, M. G. Kanatzidis, *J. Am. Chem. Soc.* **2014**, 136, 8094.
- [5] M. Hu, C. Bi, Y. Yuan, Y. Bai, J. Huang, *Adv. Sci.* **2015**, 3, 1500301.
- [6] Y. Lin, B. Chen, Y. Fang, J. Zhao, C. Bao, Z. Yu, Y. Deng, P. N. Rudd, Y. Yan, Y. Yuan, J. Huang, *Nat. Commun.* **2018**, 9, 4981.
- [7] Z. Yang, A. Rajagopal, S. B. Jo, C.-C. Chueh, S. Williams, C.-C. Huang, J. K. Katakara, H. W. Hillhouse, A. K.-Y. Jen, *Nano Lett.* **2016**, 16, 7739.
- [8] Z. Yang, A. Rajagopal, C.-C. Chueh, S. B. Jo, B. Liu, T. Zhao, A. K.-Y. Jen, *Adv. Mater.* **2016**, 28, 8990.
- [9] Y. Ogomi, A. Morita, S. Tsukamoto, T. Saitho, N. Fujikawa, Q. Shen, T. Toyoda, K. Yoshino, S. S. Pandey, T. Ma, S. Hayase, *J. Phys. Chem. Lett.* **2014**, 5, 1004.
- [10] D. Zhao, C. Wang, Z. Song, Y. Yu, C. Chen, X. Zhao, K. Zhu, Y. Yan, *ACS Energy Lett.* **2018**, 3, 305.
- [11] D. Zhao, C. Chen, C. Wang, M. M. Junda, Z. Song, C. R. Grice, Y. Yu, C. Li, B. Subedi, N. J. Podraza, X. Zhao, G. Fang, R.-G. Xiong, K. Zhu, Y. Yan, *Nat. Energy* **2018**, 3, 1093.
- [12] J. Tong, Z. Song, D. H. Kim, X. Chen, C. Chen, A. F. Palmstrom, P. F. Ndione, M. O. Reese, S. P. Dunfield, O. G. Reid, J. Liu, *Science* **2019**, 364, 475.
- [13] D. Zhao, Y. Yu, C. Wang, W. Liao, N. Shrestha, C. R. Grice, A. J. Cimaroli, L. Guan, R. J. Ellingson, K. Zhu, X. Zhao, R.-G. Xiong, Y. Yan, *Nat. Energy* **2017**, 2, 17018.
- [14] D. Forgács, L. Gil-Escrig, D. Pérez-Del-Rey, C. Momblona, J. Werner, B. Niesen, C. Ballif, M. Sessolo, H. J. Bolink, *Adv. Energy Mater.* **2017**, 7, 1602121.
- [15] A. Rajagopal, Z. Yang, S. B. Jo, I. L. Braly, P. W. Liang, H. W. Hillhouse, A. K. Jen, *Adv. Mater.* **2017**, 29, 1702140.
- [16] M. Anaya, G. Lozano, M. E. Calvo, H. Míguez, *Joule* **2017**, 1, 769.

- [17] G. E. Eperon, T. Leijtens, K. A. Bush, R. Prasanna, T. Green, J. T.-W. Wang, D. P. McMeekin, G. Volonakis, R. L. Milot, R. May, A. Palmstrom, D. J. Slotcavage, R. A. Belisle, J. B. Patel, E. S. Parrott, R. J. Sutton, W. Ma, F. Moghadam, B. Conings, A. Babayigit, H.-G. Boyen, S. Bent, F. Giustino, L. M. Herz, M. B. Johnston, M. D. McGehee, H. J. Snaith, *Science* **2016**, 354, 861.
- [18] C. Wang, Z. Song, C. Li, D. Zhao, Y. Yan, *Adv. Funct. Mater.* **2019**, 29, 1808801.
- [19] G. Xu, P. Bi, S. Wang, R. Xue, J. Zhang, H. Chen, W. Chen, X. Hao, Y. Li, Y. Li, *Adv. Funct. Mater.* **2018**, 28, 1804427.
- [20] W. Liao, D. Zhao, Y. Yu, N. Shrestha, K. Ghimire, C. R. Grice, C. Wang, Y. Xiao, A. J. Cimaroli, R. J. Ellingson, N. J. Podraza, K. Zhu, R.-G. Xiong, Y. Yan, *J. Am. Chem. Soc.* **2016**, 138, 12360.
- [21] G. Kapil, T. S. Ripolles, K. Hamada, Y. Ogomi, T. Bessho, T. Kinoshita, J. Chantana, K. Yoshino, Q. Shen, T. Toyoda, T. Minemoto, T. N. Murakami, H. Segawa, S. Hayase, *Nano Lett.* **2018**, 18, 3600.
- [22] D. Chi, S. Huang, M. Zhang, S. Mu, Y. Zhao, Y. Chen, J. You, *Adv. Funct. Mater.* **2018**, 28, 1804603.
- [23] W. Ke, I. Spanopoulos, Q. Tu, I. Hadar, X. Li, G. S. Shekhawat, V. P. Dravid, M. G. Kanatzidis, *J. Am. Chem. Soc.* **2019**, 141, 8627.
- [24] G. Kapil, T. Bessho, C. H. Ng, K. Hamada, M. Pandey, M. A. Kamarudin, D. Hirotsu, T. Kinoshita, T. Minemoto, Q. Shen, T. Toyoda, T. N. Murakami, H. Segawa, S. Hayase, *ACS Energy Lett.* **2019**, 4, 1991.
- [25] S. Shao, Y. Cui, H. Duim, X. Qiu, J. Dong, G. H. Ten Brink, G. Portale, R. C. Chiechi, S. Zhang, J. Hou, M. A. Loi, *Adv. Mater.* **2018**, 30, 1803703.
- [26] T. Jiang, Z. Chen, X. Chen, X. Chen, X. Xu, T. Liu, L. Bai, D. Yang, D. Di, W. E. I. Sha, H. Zhu, Y. M. Yang, *ACS Energy Lett.* **2019**, 4, 1784.
- [27] M. Liu, Z. Chen, Y. Yang, H.-L. Yip, Y. Cao, *J. Mater. Chem. A* **2019**, 7, 17324.
- [28] C. Li, Z. Song, D. Zhao, C. Xiao, B. Subedi, N. Shrestha, M. M. Junda, C. Wang, C.-S. Jiang, M. Al-Jassim, R. J. Ellingson, N. J. Podraza, K. Zhu, Y. Yan, *Adv. Energy Mater.* **2019**, 9, 1803135.
- [29] J. Yao, T. Kirchartz, M. S. Vezie, M. A. Faist, W. Gong, Z. He, H. Wu, J. Troughton, T. Watson, D. Bryant, J. Nelson, *Phys. Rev. Appl.* **2015**, 4, 014020.
- [30] K. Kawashima, Y. Tamai, H. Ohkita, I. Osaka, K. Takimiya, *Nat. Commun.* **2015**, 6, 10085.
- [31] Y. Zhao, Q. Li, W. Zhou, Y. Hou, Y. Zhao, R. Fu, D. Yu, X. Liu, Q. Zhao, *Sol. RRL* **2018**, 3, 1800296.
- [32] S. Gupta, D. Cahen, G. Hodes, *J. Phys. Chem. C* **2018**, 122, 13926.
- [33] J. Fan, C. Liu, H. Li, C. Zhang, W. Li, Y. Mai, *ChemSusChem* **2017**, 10, 3839.
- [34] K. Yamada, R. Nishikubo, H. Oga, Y. Ogomi, S. Hayase, S. Kanno, Y. Imamura, M. Hada, A. Saeki, *ACS Photonics* **2018**, 5, 3189.
- [35] M. Ozaki, Y. Katsuki, J. Liu, T. Handa, R. Nishikubo, S. Yakumaru, Y. Hashikawa, Y. Murata, T. Saito, Y. Shimakawa, Y. Kanemitsu, A. Saeki, A. Wakamiya, *ACS Omega* **2017**, 2, 7016.
- [36] F. Gu, S. Ye, Z. Zhao, H. Rao, Z. Liu, Z. Bian, C. Huang, *Sol. RRL* **2018**, 2, 1800136.
- [37] T.-B. Song, T. Yokoyama, C. C. Stoumpos, J. Logsdon, D. H. Cao, M. R. Wasielewski, S. Aramaki, M. G. Kanatzidis, *J. Am. Chem. Soc.* **2017**, 139, 836.
- [38] R. M. I. Bandara, K. D. G. I. Jayawardena, S. O. Adeyemo, S. J. Hinder, J. A. Smith, H. M. Thirimanne, N. C. Wong, F. M. Amin, B. G. Freestone, A. J. Parnell, D. G. Lidzey, H. J. Joyce, R. A. Sporea, S. R. P. Silva, *J. Mater. Chem. C* **2019**, 7, 8389.
- [39] R. H. Bube, *J. Appl. Phys.* **1962**, 33, 1733.
- [40] T. Bu, J. Li, F. Zheng, W. Chen, X. Wen, Z. Ku, Y. Peng, J. Zhong, Y.-B. Cheng, F. Huang, *Nat. Commun.* **2018**, 9, 4609.
- [41] Y. Chen, N. Li, L. Wang, L. Li, Z. Xu, H. Jiao, P. Liu, C. Zhu, H. Zai, M. Sun, W. Zou, S. Zhang, G. Xing, X. Liu, J. Wang, D. Li, B. Huang, Q. Chen, H. Zhou, *Nat. Commun.* **2019**, 10, 1112.
- [42] M. Kim, G.-H. Kim, T. K. Lee, I. W. Choi, H. W. Choi, Y. Jo, Y. J. Yoon, J. W. Kim, J. Lee, D. Huh, H. Lee, S. K. Kwak, J. Y. Kim, D. S. Kim, *Joule* **2019**, 3, 1.
- [43] L. Ji, X. Zhang, T. Zhang, Y. Wang, F. Wang, Z. Zhong, Z. D. Chen, Z. Xiao, L. Chena, S. Li, *J. Mater. Chem. A* **2019**, 7, 9154.
- [44] W. E. I. Sha, H. Zhang, Z. S. Wang, H. L. Zhu, X. Ren, F. Lin, A. K.-Y. Jen, W. C. H. Choy, *Adv. Energy Mater.* **2018**, 8, 1701581.
- [45] W. Ke, C. C. Stoumpos, I. Spanopoulos, M. Chen, M. R. Wasielewski, M. G. Kanatzidis, *ACS Energy Lett.* **2018**, 3, 1470.